Molecular Therapy
Oncolytics
Original Article

Selective sodium iodide symporter (*NIS*) gene therapy of glioblastoma mediated by EGFR-targeted lipopolyplexes

Rebekka Spellerberg,[1] Teoman Benli-Hoppe,[2] Carolin Kitzberger,[1] Simone Berger,[2] Kathrin A. Schmohl,[1] Nathalie Schwenk,[1] Hsi-Yu Yen,[3] Christian Zach,[4] Franz Schilling,[5] Wolfgang A. Weber,[5] Roland E. Kälin,[6,7] Rainer Glass,[6,7,8] Peter J. Nelson,[1] Ernst Wagner,[2] and Christine Spitzweg[1,9]

[1]Department of Internal Medicine IV, University Hospital, LMU Munich, 81377 Munich, Germany; [2]Pharmaceutical Biotechnology, Department of Pharmacy, LMU Munich, 81377 Munich, Germany; [3]Institute of Pathology, School of Medicine, Technical University of Munich, 81675 Munich, Germany; [4]Department of Nuclear Medicine, University Hospital, LMU Munich, 81377 Munich, Germany; [5]Department of Nuclear Medicine, School of Medicine, Klinikum rechts der Isar, Technical University Munich, 81675 Munich, Germany; [6]Neurosurgical Research, Department of Neurosurgery, University Hospital, LMU Munich, 81377 Munich, Germany; [7]Walter Brendel Center of Experimental Medicine, Faculty of Medicine, LMU Munich, 81377 Munich, Germany; [8]German Cancer Consortium (DKTK), partner site 80336 Munich and German Cancer Research Center (DKFZ), 69120 Heidelberg, Germany; [9]Division of Endocrinology, Diabetes, Metabolism and Nutrition, Mayo Clinic, Rochester, MN 55905, USA

Lipo-oligomers, post-functionalized with ligands to enhance targeting, represent promising new vehicles for the tumor-specific delivery of therapeutic genes such as the sodium iodide symporter (*NIS*). Due to its iodide trapping activity, NIS is a powerful theranostic tool for diagnostic imaging and the application of therapeutic radionuclides. ^{124}I PET imaging allows non-invasive monitoring of the *in vivo* biodistribution of functional NIS expression, and application of ^{131}I enables cytoreduction. In our experimental design, we used epidermal growth factor receptor (EGFR)-targeted polyplexes (GE11) initially characterized *in vitro* using ^{125}I uptake assays. Mice bearing an orthotopic glioblastoma were treated subsequently with mono-dibenzocyclooctyne (DBCO)-PEG$_{24}$-GE11/NIS or bisDBCO-PEG$_{24}$-GE11/NIS, and 24–48 h later, ^{124}I uptake was assessed by positron emission tomography (PET) imaging. The best-performing polyplex in the imaging studies was then selected for ^{131}I therapy studies. The *in vitro* studies showed EGFR-dependent and NIS-specific transfection efficiency of the polyplexes. The injection of monoDBCO-PEG$_{24}$-GE11/NIS polyplexes 48 h before ^{124}I application was characterized to be the optimal regime in the imaging studies and was therefore used for an ^{131}I therapy study, showing a significant decrease in tumor growth and a significant extension of survival in the therapy group. These studies demonstrate the potential of EGFR-targeted polyplex-mediated *NIS* gene therapy as a new strategy for the therapy of glioblastoma.

INTRODUCTION

Glioblastoma (GBM) is a highly aggressive tumor with very limited therapeutic options. It is the most common type of malignant primary brain tumors. Currently, the median survival time after diagnosis is 12–15 months, and fewer than 5% of patients survive more than 5 years.[1,2] The current clinical treatment involves surgical resection followed by external beam radiotherapy with concurrent chemotherapy.[2] Due to the infiltrating nature of GBM, local therapies or a complete resection are rarely possible, and the clinical relapse of the tumor is usually unavoidable. Therefore, new post-operative therapeutic strategies are seen as the key for novel curative GBM treatments.[3,4]

Targeted gene therapy is a promising approach for novel therapeutics. Research in this field has been progressing for the past few decades, with the majority of clinical trials focusing on cancer gene therapy.[5] The sodium iodide symporter (*NIS*) gene is a promising, efficient, and safe therapy gene for systemic application. The NIS protein is an intrinsic plasma membrane glycoprotein, localized at the basolateral membrane of thyroid follicular cells that mediates the active uptake of iodide for thyroid hormone synthesis. Due to its iodide trapping activity, NIS is a powerful dual-function tool, with diagnostic and therapeutic applications.[6] The functional expression of NIS can be visualized by ^{123}I scintigraphy or ^{124}I or ^{18}F-tetrafluoroborate (TFB) positron emission tomography (PET) imaging.[7,8] The application of ^{131}I or ^{188}Re and their NIS-mediated accumulation in tumor tissue allow therapeutic cytoreduction through the β emission of these radionuclides. This therapeutic concept is approved, well understood and safe, and has been in routine clinical use for more than 80 years for the treatment of thyroid cancer.[9–11] In a pioneering

Received 29 May 2021; accepted 26 October 2021;
https://doi.org/10.1016/j.omto.2021.10.011.

Correspondence: Christine Spitzweg, MD, University Hospital, LMU Munich, Department of Internal Medicine IV, Marchioninistrasse 15, 81377 Munich, Germany.
E-mail: christine.spitzweg@med.uni-muenchen.de

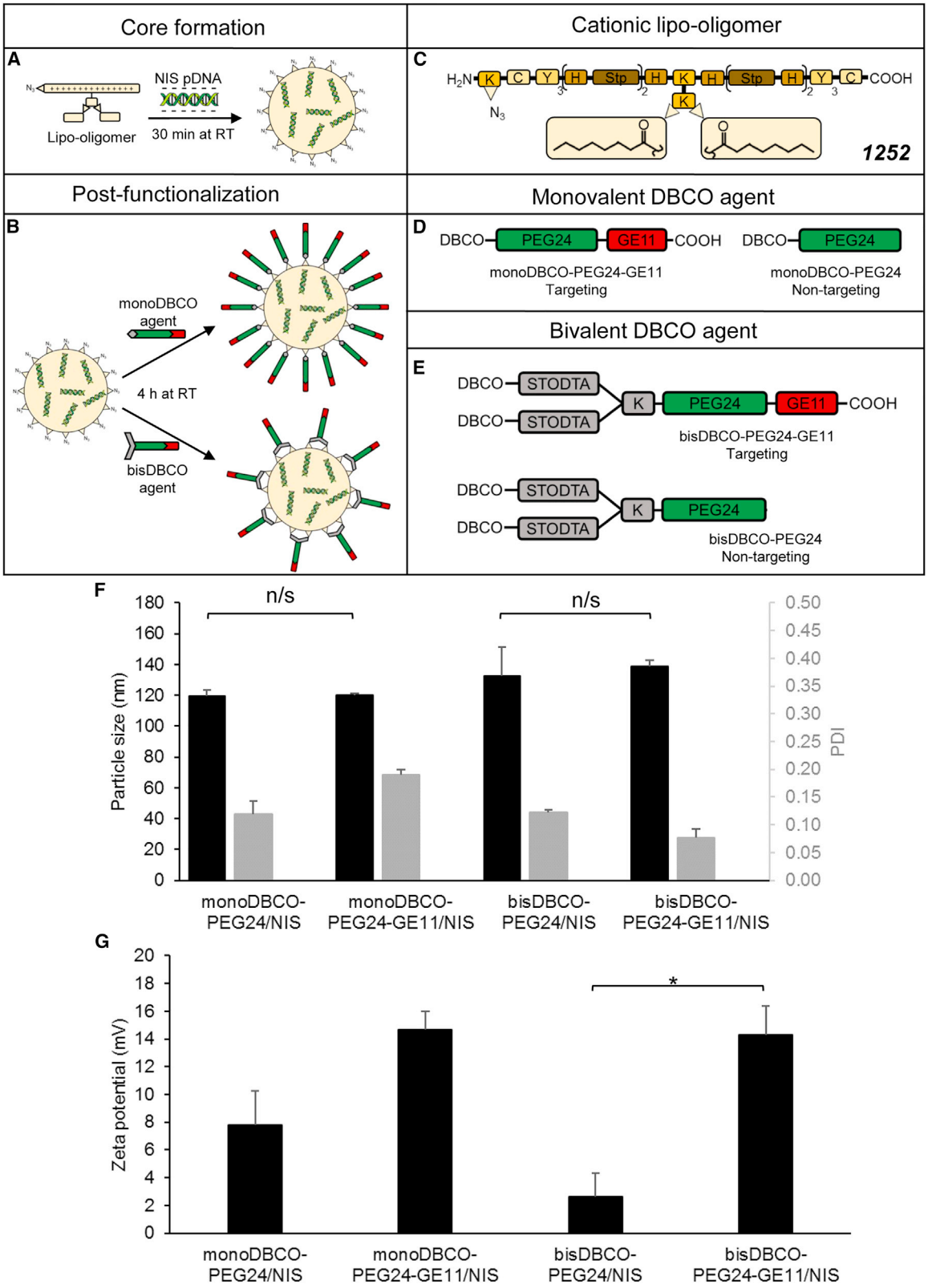

(legend on next page)

preclinical study in prostate cancer, Spitzweg *et al.* took the initial step toward human *NIS* gene transfer to non-thyroidal cancer.[12–14] In the subsequent years, multiple groups, including our own, have established new strategies and refined diverse approaches for *NIS* gene transfer into various tumor models. To this end, non-viral gene delivery represents a promising technology for the transfer of genetic material into malignant primary tumors, offering the advantages of safety, easy modification, and enhanced biocompatibility after systemic application.[15] In addition to NIS-engineered versions of mesenchymal stem cells with tumor-tissue-specific promoters for selective *NIS* gene expression,[16–25] the potential of using targeted polyplexes for the delivery of *NIS* transgenes into tumor environments has been demonstrated by several studies by our group. These include the use of polycationic molecules based on linear polyethylenimine (LPEI) that make use of the enhanced permeability and retention effect caused by the leaky vasculature found in the tumor stroma.[26,27] A PEGylated (PEG: polyethylene glycol) and epidermal growth factor receptor (EGFR)-targeted LPEI molecule (LPEI-PEG-GE11) was demonstrated to enhance tumor-specific accumulation and could be optimized by attaching targeting domains.[8,28–31] To test a broader platform of ligands targeting different tumor tissue surface receptors, ligands selectively targeting the receptor tyrosine kinase cMET and the transferrin receptor were developed.[32–34]

In the current study, we combined the theranostic *NIS* gene therapy approach with novel sequence-defined synthetic polyplexes to create an optimized, individual, and powerful treatment concept for GBM. This new generation of nanosized polyplexes is based on sequence-defined cationic lipo-oligoaminoamides (OAAs) synthesized by solid-phase assisted peptide synthesis (SPPS).[35] In addition to complexing plasmid DNA (pDNA) through electrostatic interactions, the OAA are azido-functionalized as a new feature that enables post-modification of the surface with targeting domains, to elicit an enhanced tumor-specific gene delivery. The functional azido group reacts with the dibenzocyclooctyne (DBCO) unit of potential ligands via copper-free click reaction.[36] PEGylation of the ligands lowers the surface charge to avoid non-specific aggregation or interaction with biomacromolecules, allowing an improved blood circulation and reducing undesired potential immune responses.[37,38] A monodisperse PEG_{24} (24 ethylene oxide units) was selected, which was already found to be suitable for the *in vivo* targeting of related OAA-PEG-peptide conjugates.[33,39,40] The previously established dodecapeptide GE11, a highly specific allosteric EGFR ligand, conjugated to DBCO was used.[41] EGFR is an attractive candidate for GBM targeting as its overexpression is a histopathological hallmark of GBM. In GBM development, EGFR is the most frequently amplified receptor tyrosine kinase and the receptor expression occurs early in the tumorigenesis.[42,43] The peptide GE11 was selected for EGFR targeting based on its convincingly demonstrated capacity to provide EGFR-specific transfection efficiency in nanoparticle delivery both *in vitro* and *in vivo* in our previous studies.[8,28–31,44–48] In the present study, we monitored vector biodistribution and transfection efficiency by non-invasive imaging in an orthotopic GBM mouse model and subsequently demonstrated the potential therapeutic efficacy of our novel GE11-targeted NIS polyplexes after ^{131}I application.

RESULTS

Polyplex characterization

NIS polyplexes (Figures 1A–1E) were formed with 200 μg/mL pDNA (*in vivo* conditions) and particle sizes were measured by dynamic light scattering (DLS). We aimed at a size of <200 nm to ensure unhindered blood circulation after intravenous (i.v.) injection and a sufficient cellular uptake.[49] The approximate dimensions were 120–140 nm and the polydispersity indexes (PDIs), an indicator of the heterogeneity of particle sizes in a mixture, were all below 0.2, which reflects a uniform and narrow size distribution (Figure 1F). The particle sizes did not differ significantly between targeted (monoDBCO-PEG_{24}-GE11/NIS, bisDBCO-PEG_{24}-GE11/NIS) and their corresponding non-targeted polyplexes (monoDBCO-PEG_{24}/NIS, bisDBCO-PEG_{24}/NIS). Zeta potential measurements were performed to determine the surface charge of the polyplexes. A positive surface charge is achieved through the good nucleic acid compaction of the OAAs and is desirable to ensure sufficient interaction with negatively charged cell membranes and subsequent internalization.[50] However, at the same time, it is a balancing act to prevent undesired aggregation with negatively charged macromolecules in the bioenvironment.[35] Taken together, a slightly positive surface charge is optimal. The zeta potentials of both PEGylated polyplexes (monoDBCO-PEG_{24}/NIS and bisDBCO-PEG_{24}/NIS) differed from those of GE11-targeted polyplexes (monoDBCO-PEG_{24}-GE11/NIS and bisDBCO-PEG_{24}-GE11/NIS). Using DBCO agents containing just the shielding domain (PEG_{24}) is more efficient in lowering the surface charge compared with using ligands with a shielding and a targeting domain (PEG_{24} + GE11). No formulation exceeded a zeta potential of 20 mV (Figure 1G).

In vitro NIS gene transfer mediated by EGFR-targeted polyplexes

Cell-surface EGFR expression levels were determined on human breast cancer cells MCF-7, human follicular thyroid carcinoma cells FTC-133,

Figure 1. Formulation of functionalized polyplexes

The cationic lipo-OAA containing an N-terminal azido group was mixed with pDNA at N/P 12 and incubated for 30 min at room temperature (A). Following the addition of a DBCO agent with 0.25 equivalents, another incubation for 4 h at room temperature was performed (B). Schematic depictions are shown of the sequence-defined lipo-OAA with the compound ID ***1252*** (K, lysine; C, cysteine; Y, tyrosine; H, histidine; Stp, succinoyltetraethylene-pentamine) (C) and the structure of PEGylation agents for post-functionalization containing monovalent (D) or bivalent (E) DBCO with ligand peptide GE11 for targeting of EGFR or without GE11 as negative non-targeting control. DLS measurements of formed polyplexes revealed a size of 120–140 nm with a uniform size distribution (PDI of <0.2) (F) and a zeta potential below 20 mV, whereas non-targeted PEGylated polyplexes showed more efficient surface shielding than polyplexes with targeted ligands (G) (*$p \leq 0.05$; n/s, not significant). Results are reported as mean ± SEM (n = 3). RT, room temperature.

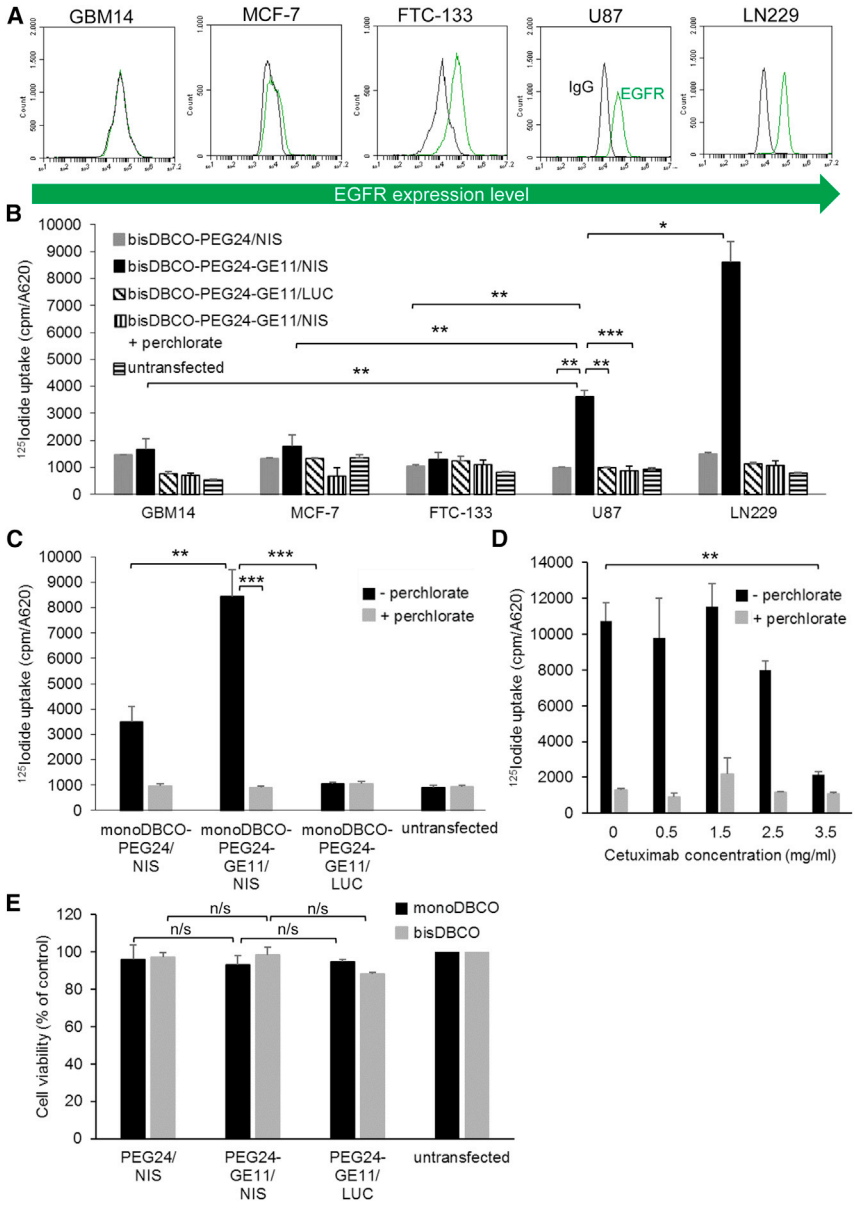

Figure 2. EGFR-targeted *NIS* gene transfer *in vitro*

Cell-surface expression of EGFR was measured by flow cytometry. A specific antibody detected the expression levels of human EGFR on GBM14, MCF-7, FTC-133, U87, and LN229 compared with isotype controls (A). ^{125}I transfection studies with GBM14, MCF-7, FTC-133, U87, and LN229 (n = 3) indicate a correlation between the receptor expression levels and the transfection efficiency of targeted polyplexes (bisDBCO-PEG$_{24}$-GE11/NIS) (B). Receptor specificity was shown by transfecting cells with untargeted polyplexes (monoDBCO-PEG$_{24}$/NIS n = 6 and bisDBCO-PEG$_{24}$/NIS n = 3), resulting in a significantly lower iodide uptake. Background radiation levels after control transfection with LUC-coding polyplexes (monoDBCO-PEG$_{24}$-GE11/LUC n = 6 and bisDBCO-PEG$_{24}$-GE11/LUC n = 3) or the addition of NIS-specific inhibitor perchlorate prove NIS dependency of iodide uptake (B and C) (*p ≤ 0.05, **p ≤ 0.01, ***p ≤ 0.001). Treatment with the selective EGFR inhibitor cetuximab resulted in a dose-dependent inhibition of the transfection of U87 cells using monoDBCO-PEG$_{24}$-GE11/NIS polyplexes, demonstrating the EGFR dependency of transfection with GE11 polyplexes (D) (**p ≤ 0.01). Cell viability of U87 was affected neither by monoDBCO- nor by bisDBCO-polyplex treatment (E). Results are reported as mean ± SEM.

and the human GBM cell lines GBM14, U87, and LN229 by flow cytometry. GBM14 cells showed no EGFR expression, MCF-7 a very low expression level, FTC-133 a low level of EGFR expression, and LN229 cells the highest EGFR density on their surface. U87 expressed an intermediate level of EGFR (Figure 2A). The results indicate that the EGFR expression levels on the cells correlated with transfection efficiency after transfection with bisDBCO-PEG$_{24}$-GE11/NIS polyplexes. LN229 cells showed significantly higher ^{125}I uptake than U87 cells, while no EGFR-expressing GBM14, very low EGFR-expressing MCF-7, and low EGFR-expressing FTC-133 cells exhibited a significantly lower ^{125}I uptake (Figure 2B). The transfection efficiency was higher in U87 and LN229 cells using the targeting ligand GE11: transfection of U87 with bisDBCO-PEG$_{24}$-GE11/NIS polyplexes resulted in a 4-fold increase in ^{125}I uptake after 24 h compared with transfection with non-targeting bisDBCO-PEG$_{24}$/NIS polyplexes (Figure 2B). Transfection of U87 with monoDBCO-PEG$_{24}$-GE11/NIS polyplexes led to a 2.5-fold increase in ^{125}I uptake compared with non-targeting monoDBCO-PEG$_{24}$/NIS polyplexes (Figure 2C). The transfection of U87 with monoDBCO-PEG$_{24}$-GE11/NIS resulted in higher iodide uptake levels compared with the transfection with bisDBCO-PEG$_{24}$-GE11/NIS, indicating a higher efficiency of the monoDBCO-PEG$_{24}$-GE11/NIS polyplexes (Figures 2B and 2C). In all cell lines, the addition of the NIS-specific inhibitor perchlorate blocked ^{125}I uptake in NIS-transfected cells, and no iodide uptake above background was seen using luciferase (LUC)-coding polyplexes (Figures 2B and 2C). To further validate the EGFR-dependent transfection efficiency, U87 cells were treated simultaneously with increasing concentrations of the selective EGFR inhibitor cetuximab and monoDBCO-PEG$_{24}$-GE11/NIS polyplexes. A decrease in radioiodide uptake was shown at 2.5 mg/mL cetuximab with a complete inhibition of radioiodide uptake activity at 3.5 mg/mL cetuximab (Figure 2D). All results were normalized to cell survival and U87 cell viability was not affected by polyplex treatment (Figure 2E).

Tumoral iodide uptake *in vivo* after systemic *NIS* gene transfer

To determine EGFR expression levels, tissue samples from an orthotopic U87 GBM xenograft mouse model (Figure 3A) were stained

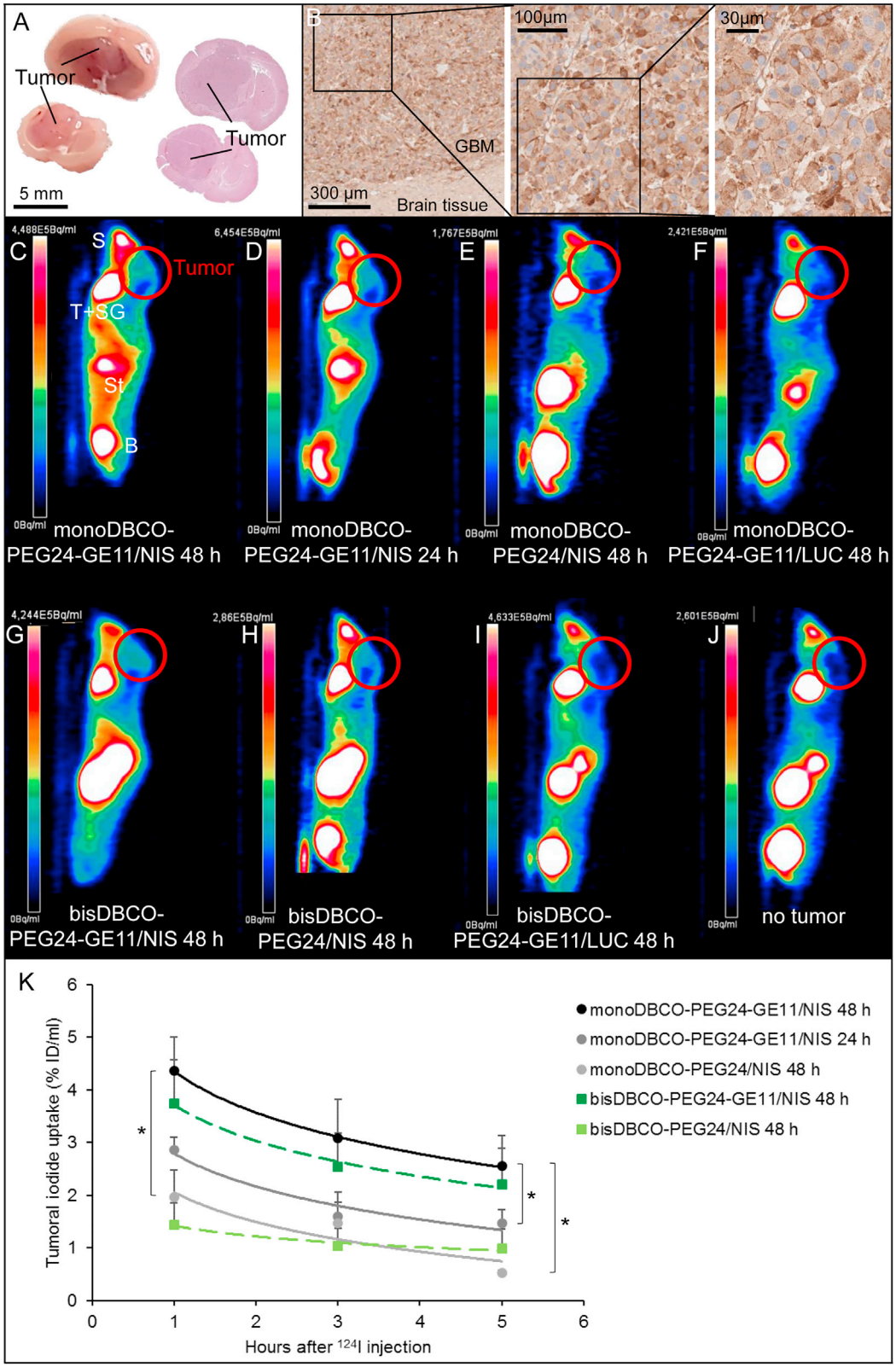

(legend on next page)

using specific antibodies. All tumors (n = 7) were EGFR positive, with up to 40% positive cells per tumor (Figure 3B). GBM-bearing mice received EGFR-targeted polyplexes systemically and were evaluated for functional NIS expression in the tumor tissue. Polyplex injection was scheduled 24–28 days after intracranial (i.c.) tumor cell inoculation and 24 or 48 h later high-resolution ^{124}I PET imaging was performed to quantify tumoral radioiodide uptake. The contrast between high radioiodide uptake in the tumors of mice treated with EGFR-targeted polyplexes (Figures 3C, 3D, and 3G) and low tumoral radionuclide uptake in mice injected with non-targeted polyplexes (Figures 3E and 3H) is indicated by the differences in signal strength. No tumoral iodide uptake above background (Figure 3J) was measured in mice that received LUC-coding polyplexes (Figures 3F and 3I). Due to physiological NIS expression, the thyroid, salivary glands, and stomach normally accumulate radioiodide. The bladder also contains radioiodide due to renal elimination (Figure 3C–3J).

In the quantitative analysis, tumors of mice that received monoDBCO-PEG$_{24}$-GE11/NIS showed a significantly higher ^{124}I uptake of 4.36 ± 0.65% ID/mL (48 h) and 2.86 ± 0.24% ID/mL (24 h) compared with tumors from mice that received non-targeted monoDBCO-PEG$_{24}$/NIS polyplexes, which exhibited an uptake of 1.96 ± 0.52% ID/mL.

Measurements in mice that received bisDBCO-PEG$_{24}$-GE11/NIS confirmed the advantageous effect of EGFR-targeted compared with non-targeted polyplexes. With a tumoral iodide uptake of 3.74 ± 0.83% ID/mL, the cohort pretreated with bisDBCO-PEG$_{24}$-GE11/NIS showed a higher signal amplification than the group injected with bisDBCO-PEG$_{24}$/NIS (1.44 ± 0.42% ID/mL) (Figure 3K).

Considering a tumor mass of 0.1 g, dosimetric calculations revealed the highest tumor-absorbed dose of 58.0 ± 18.3 mGy/MBq ^{131}I with an effective half-life of 9.6 h in the mice treated with monoDBCO-PEG$_{24}$-GE11/NIS followed by radioiodide 48 h later. For mice treated with non-targeted polyplexes (monoDBCO-PEG$_{24}$/NIS), a dose of 8.2 ± 1.0 mGy/MBq and an effective half-life of 2.9 h for ^{131}I were calculated. A dose of 35.0 ± 14.2 mGy/MBq ^{131}I and an effective half-life of 5.4 h were determined for the bisDBCO-PEG$_{24}$-GE11/NIS group. Matching the *in vitro* data, monoDBCO-PEG$_{24}$-GE11/NIS polyplexes resulted in a higher tumoral iodide uptake and a higher tumor-absorbed dose compared with the bisDBCO-PEG$_{24}$-GE11/NIS polyplexes, corroborating the greater transfection efficiency of the monoDBCO-PEG$_{24}$-GE11/NIS polyplexes, as a basis for their application in the *in vivo* therapy study.

Immunohistochemical *ex vivo* analysis of NIS protein expression

After tissue preparation, sections were stained immunohistochemically using an anti-NIS monoclonal antibody. Tumor sections derived from mice that received monoDBCO-PEG$_{24}$-GE11/NIS polyplexes 48 h (Figure 4A) before sacrifice showed a higher number of NIS-positive cells (red) than tumor sections from the 24h group (Figure 4B). Immunohistochemical staining of tumor sections from control animals that received non-targeted monoDBCO-PEG$_{24}$/NIS (Figure 4C) or LUC-coding monoDBCO-PEG$_{24}$-GE11/LUC (Figure 4D) polyplexes showed no NIS-specific immunoreactivity that was comparable to untreated (Figure 4E) tumor tissue.

Immunohistochemical NIS staining of tumor sections derived from mice treated with bisDBCO-PEG$_{24}$-GE11/NIS (Figure 4F) polyplexes demonstrated an analogous outcome. The experimental group revealed clusters of NIS-positive cells, in contrast with control groups bisDBCO-PEG$_{24}$/NIS (Figure 4G) and bisDBCO-PEG$_{24}$-GE11/LUC (Figure 4H), which showed no NIS detection.

In tissue sections of control organs (liver [Figure 4I], lung [Figure 4J], kidney [Figure 4K], and spleen [Figure 4L]), no NIS expression was detected.

^{131}I therapy studies after polyplex-mediated *NIS* gene transfer *in vivo*

Based on the results of the imaging studies, GBM bearing mice were then treated with monoDBCO-PEG$_{24}$-GE11/NIS followed by ^{131}I application 48 h later (therapy group). This application cycle was repeated three times. Control groups concurrently received non-targeting monoDBCO-PEG$_{24}$/NIS polyplexes followed by ^{131}I or monoDBCO-PEG$_{24}$-GE11/NIS polyplexes and then NaCl or NaCl only as a negative control. Tumor growth was monitored by high-resolution magnetic resonance imaging (MRI) twice a week. The therapy group (Figure 5A) showed a significant delay in tumor growth compared with the control groups. The tumor growth was only mildly decreased in the group monoDBCO-PEG$_{24}$/NIS followed by ^{131}I (Figure 5B) and an aggressive tumor growth was observed in the two control groups, namely, monoDBCO-PEG$_{24}$-GE11/NIS plus NaCl (Figure 5C) and NaCl only (Figure 5D). The enhanced therapy effect seen in tumor growth (Figure 5E) resulted in a significant extension of survival of the therapy group (Figure 5F).

Figure 3. Polyplex-mediated *NIS* gene transfer *in vivo*

U87 GBM (A) showed high membranous EGFR expression in the receptor staining compared with no EGFR expression in normal brain tissue (B). Original magnifications of 8× (scale bar: 300 μm), 15× (scale bar: 100 μm), and 40× (scale bar: 30 μm) were chosen. Tumoral iodide uptake in ^{124}I PET studies was significantly higher in mice treated with monoDBCO-PEG24-GE11/NIS (n = 5) (C) compared with non-targeting monoDBCO-PEG24/NIS (n = 4) (E). No tumoral iodide uptake above background was measured in mice that received LUC-coding monoDBCO-PEG24-GE11/LUC polyplexes (n = 3) (F), comparable to mice that did not bear a tumor (J). An interval of 48 h between systemic polyplex injection and iodide administration resulted in a higher iodide uptake than an interval of 24 h (n = 5) (C, D). Analogous outcomes and reproduction of the advantageous targeting effect of GE11 polyplexes were seen in studies with bisDBCO-PEG24-GE11/NIS (n = 5) (G) for targeted, bisDBCO-PEG24/NIS (n = 3) (H) for non-targeted, and bisDBCO-PEG24-GE11/LUC (n = 2) (I) for LUC-coding polyplexes. One representative image is shown for each group. Tumoral iodide uptake was measured by serial scannings over 5 h and quantified as the percentage of the injected dose per milliliter tumor (K) (*$p \leq 0.05$). Results are reported as mean ± SEM (S, snout, nasal secretion; T, thyroid; SG, salivary glands; St, stomach; B, bladder).

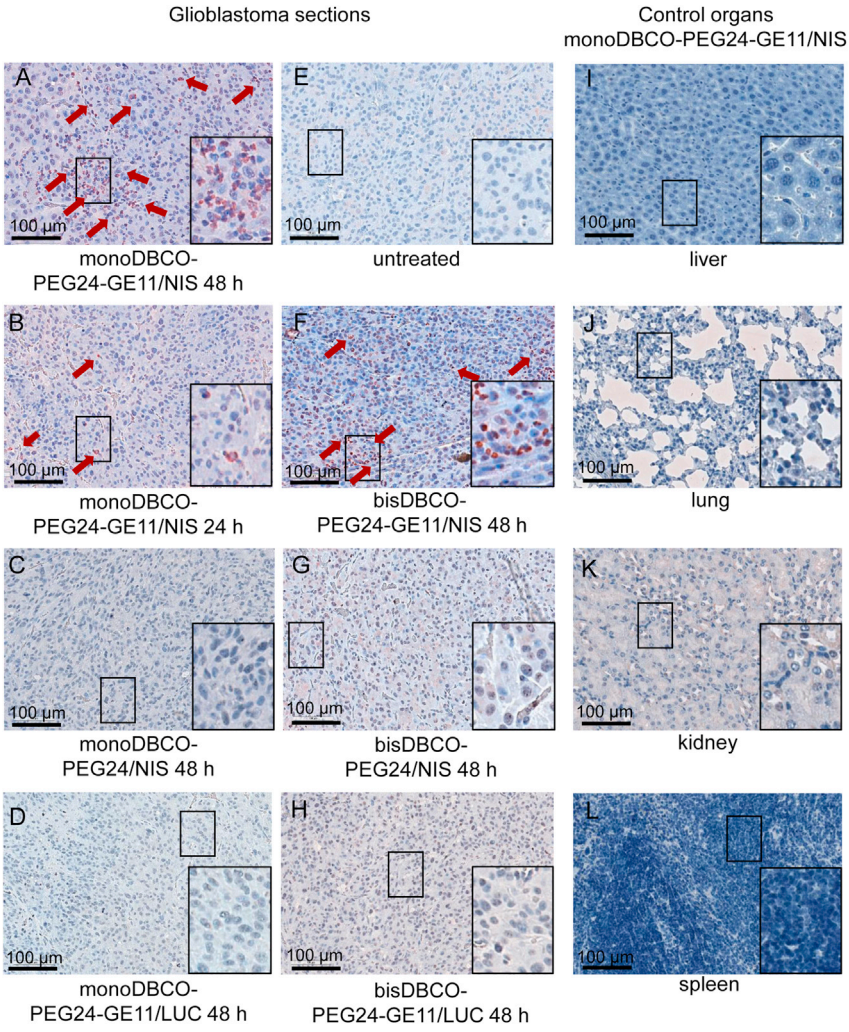

Figure 4. Analysis of NIS protein expression in U87 tumors *ex vivo*

Immunohistochemical staining of NIS protein in GBM xenografts embedded in paraffin revealed a higher NIS expression (red) in mice treated with targeted polyplexes (monoDBCO-PEG_{24}-GE11/NIS [A] and bisDBCO-PEG_{24}-GE11/NIS [F]) 48 h before sacrifice compared with the 24h time point (B). No positive NIS staining in tumors of mice that received control polyplexes (C, D, G, and H) or untreated (E) mice was observed. Liver (I), lung (J), kidney (K), and spleen (L) did not show any NIS expression. One representative image with 20× original magnification is shown for each group (scale bar: 100 µm). A 40× original magnification was chosen for the close up (scale bar: 50 µm).

On day 26, the last control mouse was sacrificed based on the animal welfare protocol, while 60% of the therapy mice were still alive. The mean survival times were 26.6 days for the therapy group, 22.6 days for the monoDBCO-PEG_{24}/NIS + ^{131}I group, 20.4 days for the monoDBCO-PEG_{24}-GE11/NIS + NaCl group, and 20 days for the NaCl-only group.

The results were further validated by staining of the blood vessel density and proliferation status (Figures 6A–6D). The therapy group showed a trend toward the lowest number of Ki67-positive cells (Figure 6E) and a significantly smaller area of CD31 positivity (Figure 6F) compared with the control groups.

DISCUSSION

As the most common malignant primary brain tumor, GBM has an incidence of 3.19 cases per 100,000 person years.[51] The remarkably poor prognosis of 15 months median survival[52] results from very limited treatment options and the diffuse-invasive nature of GBM with a remaining poor understanding of tumor pathophysiology.[52,53] The current therapeutic strategy is multidisciplinary. Diagnostic procedures involve MRI scan and biopsy, whereas therapy involves surgical resection followed by adjuvant therapies. The gold standard of post-operative strategies is radiation therapy combined with the alkylating agent temozolomide.[52,54] For recurrent disease that is progressive despite prior therapy, the monoclonal antibody bevacizumab was authorized by the US Food and Drug Administration (FDA).[55] T cell inhibitors, peptide- and dendritic cell-based vaccination, adoptive cell therapy, and viral immunotherapy are new approaches currently in clinical phase studies for GBM, but have not been approved by the FDA or EMA yet. To date, these therapeutic approaches do not differ much regarding prognosis and overall survival,[51] highlighting the need for new strategies.

The cloning of *NIS* in 1996 opened up the opportunity of using this theranostic gene for non-invasive imaging and therapy purposes.[56] Due to its origin in thyroid follicular cells, it is a self-protein with no immunogenic potential and no cell toxicity.[11] In addition to scintigraphic imaging, NIS facilitates tumor monitoring by PET using ^{124}I or ^{18}F-TFB as tracers.[7,8] PET allows for the quantitative analysis of tumoral iodide uptake mediated by functional NIS expression with a high resolution and sensitivity and allows a three-dimensional reconstruction of tumors. NIS imaging allows a precise estimation of radiation dose for radioablation of the individual tumor based on dosimetric calculations.[57] Applying ^{131}I leads to radionuclide trapping within the NIS-positive cells and cell death induced by beta decay. The cross-fire effect further boosts the impact of ^{131}I, as neighboring cells also suffer cytotoxic destruction.[58] Off-target toxicity affects mainly the thyroid and salivary glands due to their physiologic NIS expression. Pretreatment with LT4 causes a downregulation of thyroidal iodide uptake due to the TSH dependency of NIS expression. Should hypothyroidism nonetheless arise after therapy, it can be treated by thyroid hormone substitution.[11] The efficacy of radioiodide therapy is well established in thyroid cancer treatment, even in advanced metastatic disease.[59]

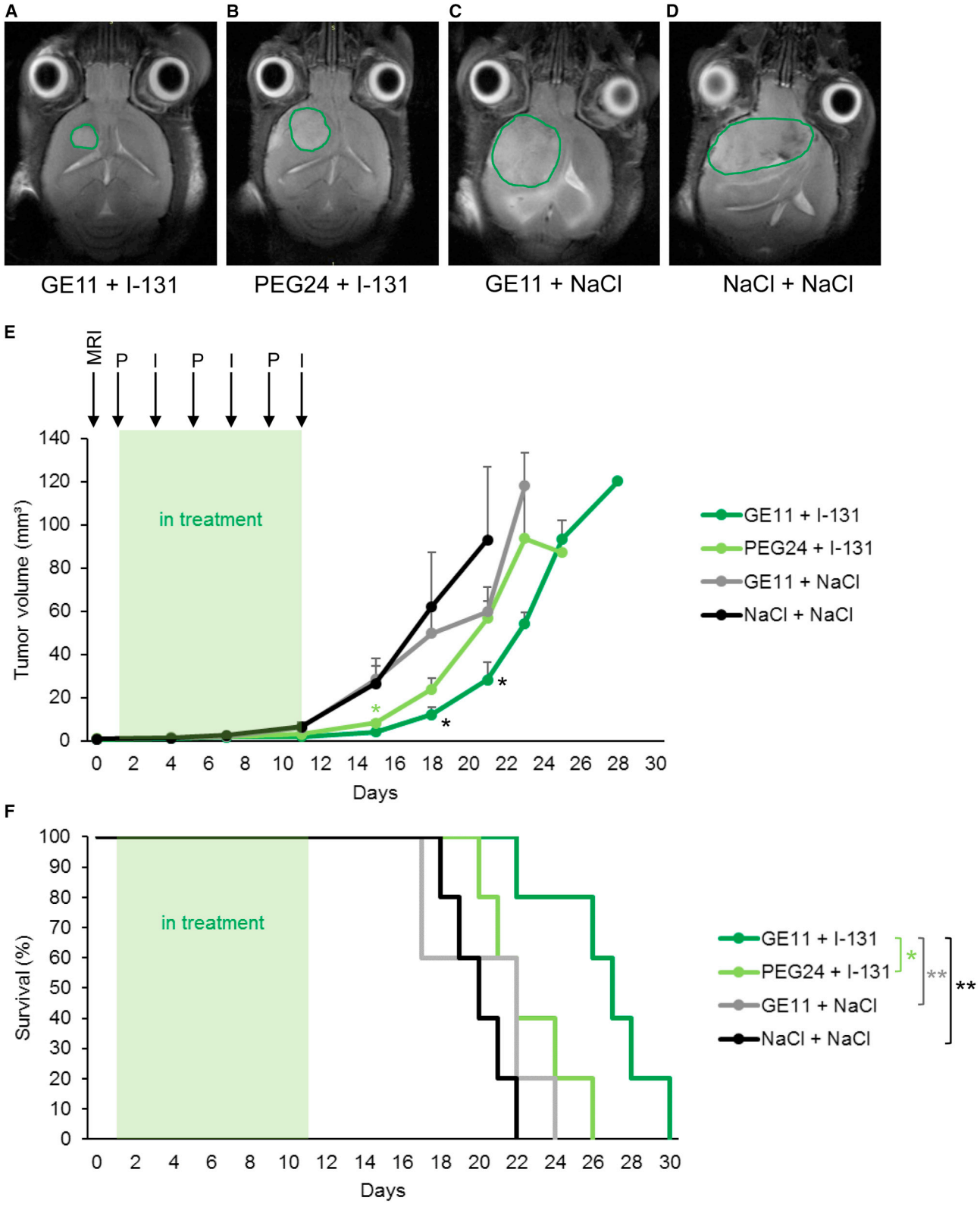

(legend on next page)

This therapeutic effectiveness empowers the potential translation of NIS-mediated radioiodide therapy to other tumor diseases such as GBM. In the past, Cho *et al.*[60] showed functional NIS expression in subcutaneous glioma tumors after intratumoral injection of NIS-expressing recombinant adenoviruses. In a further step, Opyrchal *et al.*[61] have shown a prolonged survival of orthotopic GBM-bearing mice treated with intratumoral injection of measles virus engineered to express NIS followed by the intraperitoneal (i.p.) injection of ^{131}I compared with the MV-NIS-only group. In the present study, we used sequence-defined polyplexes as artificial virus-like carrier systems. These synthetic carriers may have distinct advantages over viral vectors, as they overcome limitations in virus gene therapies such as immunogenicity, limited cargo capacity, and difficulties in production.[62] But, at the same time, this technology is inspired by virus biology in that they allow targeted, dynamic, and potent nucleic acid delivery.[37] Importantly, in our study, we injected polyplexes systemically instead of intratumorally, highlighting the flexibility of this approach in clinical applicability. Critical parameters for polyplexes are size, charge, and surface characteristics. The T-shaped lipo-OAA ***1252*** packages the NIS pDNA and is responsible for the balance between stability and endosomal release.[63] Very small polyplexes (<6 nm) are rapidly eliminated by the kidney, while very big polyplexes (>400 nm) need extensive vascularization for their accumulation in solid tumors.[35] Our polyplexes have been designed for a size between 120 and 140 nm for optimal biodistribution and pharmacokinetics. Modification with the PEGylated ligands resulted in surface charges below 20 mV. This might be advantageous in view of avoiding self-aggregation and aggregation with biomacromolecules and to provide longer blood circulation (Figure 1).[35] Size and charge influence non-specific accumulation in the liver, lungs, and kidneys, which can create toxicity issues.[57] In *ex vivo* immunohistochemical stainings, we found no NIS expression in these healthy organs (Figures 6I–6L). To increase the internalization of our synthetic vectors to tumor stroma, we used GE11 ligands for specific tumor targeting.[31] We further showed EGFR-dependent transfection efficiency *in vitro* and *in vivo*. The comparison of targeted polyplexes (monoDBCO-PEG$_{24}$-GE11/NIS and bisDBCO-PEG$_{24}$-GE11/NIS) with their corresponding non-targeted polyplexes (monoDBCO-PEG$_{24}$/NIS and bisDBCO-PEG$_{24}$/NIS) demonstrated the advantageous effect of using GE11 targeting ligands. In *in vitro* cell transfection (Figure 2) and *in vivo* PET imaging experiments (Figure 3), the use of GE11 ligands led to a significantly higher transfection efficiency compared with the PEG$_{24}$ ligands alone. Transfection resulted in background levels when using LUC-coding polyplexes (monoDBCO-PEG$_{24}$-GE11/LUC and bisDBCO-PEG$_{24}$-GE11/LUC), thus demonstrating that iodide uptake is indeed NIS mediated. The outcome of our therapy study matched closely the results of the PET imaging study. The effective therapeutic cytoreduction achieved after treatment with targeted monoDBCO-PEG$_{24}$-GE11/NIS polyplexes followed by ^{131}I application resulted in a significant decrease in tumor growth compared with the two control groups monoDBCO-PEG$_{24}$-GE11/NIS plus NaCl and NaCl only. The non-targeted polyplexes (monoDBCO-PEG$_{24}$/NIS) showed an uptake of ^{124}I only slightly above background levels in the imaging study. Accordingly, mice treated with these non-targeted polyplexes followed by ^{131}I in the therapy study showed a mild delay in tumor growth compared with the other two control groups. These observations in tumor growth behavior during therapy were mirrored by animal survival (Figure 5). The *ex vivo* analysis of NIS protein expression showed a heterogeneous, patchy transgene expression pattern *in vivo* after polyplex-mediated transfection (Figures 4A and 4F). Nevertheless, the ^{131}I therapy resulted in a significant therapeutic effect. This outcome is attributed to the bystander effect of the beta-emitter ^{131}I, which is able to compensate heterogeneous tumoral NIS expression due to the range of approximately 2.4 mm of the beta particles.[10,17,64,65] This is one of the major advantages of *NIS* as a therapy gene and makes the approach highly effective.[66] *Ex vivo* staining for blood vessel density demonstrated a long-term antiangiogenic therapeutic effect of ^{131}I treatment. The vascularization status of a tumor influences the growth rate. A highly vascularized tumor grows more rapidly, whereas low vascularization decelerates tumor growth.[67] The tumors of the therapy group showed the lowest blood vessel density, delayed growth, and a trend toward lower cell proliferation as determined by Ki67 staining (Figure 6).

In summary, our work clearly shows the potential of post-functionalized targeted polyplexes for *NIS* gene therapy of GBM using the EGFR targeting ligand GE11. During the last decade, it has been shown that GBMs comprise a group of highly heterogeneous tumor types, including mutations, rearrangements, and genetic alterations of EGFR.[43] EGFR amplification is acquired by GBM cells early in tumorigenesis and substantially contributes to the invasive process.[43] In a study by van den Bent *et al.*, approximately 84% of the evaluated GBMs were considered to retain their EGFR amplification at the time of tumor recurrence.[68] As amplification of tumoral EGFR is essential for the success of our personalized therapy approach, EGFR expression is optimally assessed pre-therapeutically as part of the molecular tumor profiling. The theranostic approach of the *NIS* gene therapy offers the major advantage of non-invasive monitoring of the efficacy of EGFR-targeted *NIS* gene delivery

Figure 5. ^{131}I therapy studies *in vivo*

GBM-bearing mice, confirmed by MRI on day 0, were treated with three cycles of i.v. injection of polyplexes on days 1, 5, and 9 followed by i.p. injection of 55.5 MBq ^{131}I 48 h later, on days 3, 7, and 11. Tumor sizes were monitored twice a week by MRI. Exemplary MRI images of tumor sizes on day 18 of the therapy trial from a monoDBCO-PEG$_{24}$-GE11/NIS + ^{131}I (A), a monoDBCO-PEG$_{24}$/NIS + ^{131}I (B), a monoDBCO-PEG$_{24}$-GE11/NIS + NaCl (C), and a NaCl + NaCl (D)-treated mouse are shown. Tumors are highlighted by green lines. Injection of monoDBCO-PEG$_{24}$-GE11/NIS + ^{131}I led to a decrease in tumor growth in the therapy group (n = 5) compared with control groups monoDBCO-PEG$_{24}$/NIS + ^{131}I (n = 5; mean ± SEM; *p < 0.05 on day 15), monoDBCO-PEG$_{24}$-GE11/NIS + NaCl (n = 5; mean ± SEM), and NaCl + NaCl (n = 5; mean ± SEM; *p < 0.05 on days 18 and 21) (E). Therapy mice treated with monoDBCO-PEG$_{24}$-GE11/NIS + ^{131}I (n = 5) showed a significant extension of survival compared with control groups monoDBCO-PEG$_{24}$/NIS + ^{131}I (n = 5; *p < 0.05), monoDBCO-PEG$_{24}$-GE11/NIS + NaCl (n = 5; **p < 0.01), and NaCl + NaCl (n = 5; **p < 0.01) (F).

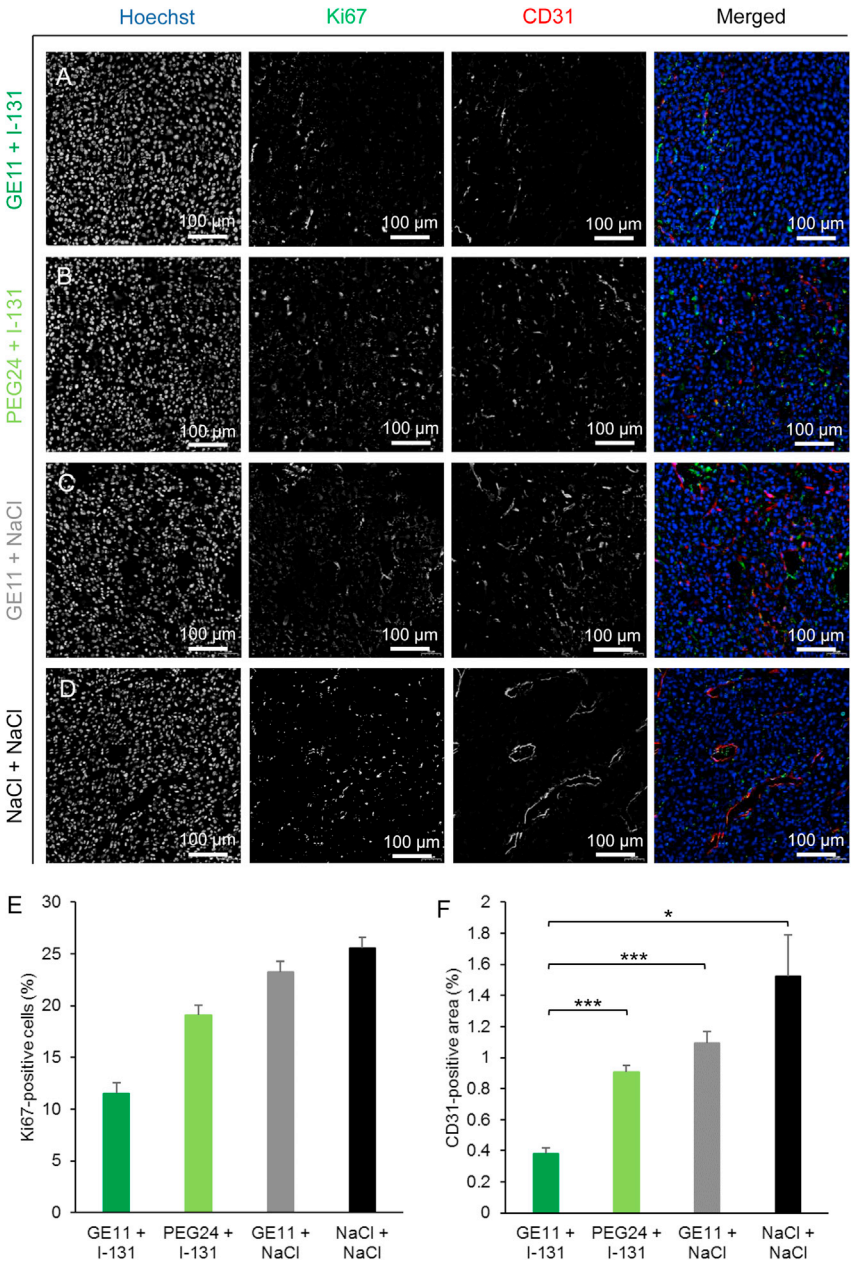

Figure 6. Analysis of proliferation index and blood vessel density of therapy tumors *ex vivo*

Frozen tissue sections from GBM dissected after the therapy study were stained for Ki67 (green) for proliferation index and CD31 (red) for blood vessel density. Nuclei are stained with Hoechst (blue). The therapy group that received monoDBCO-PEG_{24}-GE11/NIS followed by ^{131}I (A) showed fewer Ki67-positive cells (E) and a significantly smaller CD31-positive area (F) (*$p < 0.05$, ***$p < 0.001$) compared with the control groups treated with monoDBCO-PEG_{24}/NIS plus ^{131}I (B), monoDBCO-PEG_{24}-GE11/NIS plus NaCl (C), or NaCl only (D). One representative picture of each group is shown at 20× original magnification (scale bar: 100 µm). Results are reported as mean ± SEM (for each group n = 4).

before a therapeutic dose of radioiodide is applied, as demonstrated in our preclinical *in vivo* studies (Figures 3C, 3D, and 3G). Furthermore, the use of DBCO click chemistry provides the opportunity to design polyplexes quickly, based on the genetic differentiation and receptor status of the individual tumor. After biopsy and analysis of the molecular tumor profile, the polyplex design can be tailored via the targeting domain to provide a personalized and individual therapy. The application of alternative targeting ligands suitable for DBCO click chemistry is the subject of ongoing work and can provide a broad spectrum of polyplexes for individualized therapy.

MATERIALS AND METHODS

Cell culture

The GBM cell line U87 (CLS 300367, Cell Line Service GmbH, Eppelheim, Germany) was cultured in Dulbecco's modified Eagle's medium (DMEM; 1 g/L glucose; Sigma Aldrich, St. Louis, MO) supplemented with 1% (v/v) MEM non-essential amino acids (Thermo Fisher Scientific, Waltham, MA). The GBM cell line LN229 (ATCC CRL-2611, American Type Culture Collection, Manassas, VA) was grown in Roswell Park Memorial Institute (RPMI)-1640 culture medium (Sigma Aldrich) supplemented with 1% (v/v) sodium pyruvate (Thermo Fisher Scientific). The follicular thyroid carcinoma cell line FTC-133 (94,060,902, Sigma Aldrich) was cultured in DMEM/F12 (Sigma Aldrich) supplemented with 1% (v/v) L-glutamine (Sigma Aldrich). The human breast cancer cell line MCF-7 (ATCC HTB-22) was grown in minimum essential Eagle's medium (MEM; Sigma Aldrich) supplemented with 1% (v/v) L-glutamine (Sigma Aldrich), 1% (v/v) sodium pyruvate (Thermo Fisher Scientific), and 5 µg/mL insulin (Sigma Aldrich). We added 10% (v/v) fetal bovine serum (FBS Superior, Sigma Aldrich) and 1% (v/v) penicillin/streptomycin (Sigma Aldrich) to all media. The patient-derived GBM cell line GBM14 was cultured in DMEM/F12 (Sigma Aldrich) supplemented with 1% (v/v) penicillin/streptomycin (Sigma Aldrich), B-27 supplement (Thermo Fisher Scientific), 10 ng/mL human EGF (PeproTech, Hamburg, Germany), and 10 ng/mL human FGF (PeproTech). All cells were passaged at 70% confluency and maintained at 37°C, 5% CO_2, and a relative humidity of 95%. The culture medium was replaced every 48 h.

Synthesis of plasmids, carrier, and DBCO agents

The NIS cDNA was synthesized and optimized by GENEART (Regensburg, Germany) based on the plasmid pCpG-hCMV-Luc. The

establishment of the expression vector pCpG-hCMV-NIS has been described in detail previously.[29] The pNIS-DNA and pCMVLuc[69] (encoding a *Photinus pyralis* LUC under control of the cytomegalovirus promoter) that were applied in all *in vitro* and *in vivo* experiments were produced and purified by Plasmid Factory GmbH (Bielefeld, Germany).

The T-shaped OAA ***1252*** was synthesized via standard Fmoc SPPS as described previously.[45,63]

The shielding and EGFR targeting agents, bearing one or two DBCO units as attachment sites for orthogonal click reaction, were synthesized as described previously.[45,47]

Polyplex formation

The final pDNA concentration was 10 μg/mL for cell transfection experiments and 200 μg/mL for *in vivo* experiments. The pDNA and the calculated amount of OAA at N/P 12 (protonatable nitrogen/phosphate ratio) were diluted separately in the same volume. The solvent was 20 mM HEPES buffer with 5% (w/v) glucose (pH 7.4) (HBG buffer). The pDNA solution was mixed in OAA solution by pipetting rapidly 10 times, followed by an incubation period of 30 min at room temperature to form core polyplexes. Ligands for post-modification were diluted in HBG buffer with an equivalence of 0.25.[36] The total volume of the diluted ligand was one-quarter of the volume of the OAA-pDNA mixture. The ligand was added to the core polyplex solution after the incubation period by pipetting rapidly 10 times, followed by further incubation for 4 h at room temperature.

Particle size and zeta potential measurement

DLS was performed on a Zetasizer Nano ZS (Malvern Instruments, Worcestershire, UK) to measure the particle size and zeta potential of the polyplexes. Polyplexes were formed in 100 μL HBG buffer with a final DNA concentration of 200 μg/mL (*in vivo* condition). For zeta potential measurement, 700 μL HBG was added.

EGFR expression levels *in vitro*

Flow cytometry was performed to screen for EGFR expression levels on cell surfaces. U87, LN229, MCF-7, and FTC-133 were trypsinized and GBM14 was treated with Accutase solution (Sigma Aldrich). We washed 8×10^5 cells of each cell line and resuspended them in 100 μL PBS supplemented with 10% (v/v) FBS (FACS buffer). An antibody for human EGFR detection (monoclonal mouse IgG1, clone H11; Dako, Glostrup, Denmark) or a negative isotype control antibody (Abcam, Cambridge, UK) was added at a dilution of 1:200 and the samples were incubated for 1 h on ice. Subsequently, the cells were washed with FACS buffer and stained with an Alexa Fluor 488 antibody at a dilution of 1:400 (Thermo Fisher Scientific) for 1 h on ice. Propidium iodide (Sigma Aldrich) was added at a dilution of 1:100 to exclude dead cells. An analysis was performed on a BD Accuri C6 flow cytometer (BD Bioscience, Franklin Lakes, NJ). Cell aggregates or fractions were excluded by appropriate gating.

Transfection studies and ^{125}I uptake assay

Cells (U87, LN229, GBM14, MCF-7, and FTC-133) were seeded in six-well plates and grown to 60%–70% confluency. Medium was replaced by 400 μL/well serum- and antibiotic-free medium. We added 200 μL/well monoDBCO-PEG$_{24}$-GE11/NIS or bisDBCO-PEG$_{24}$-GE11/NIS polyplex solutions with a DNA concentration of 10 μg/mL and the cells were incubated for 4 h at 37°C before the medium was changed to normal growth medium. As negative controls, ligands without the targeting domain (monoDBCO-PEG$_{24}$/NIS or bisDBCO-PEG$_{24}$/NIS) or LUC-coding polyplexes (monoDBCO-PEG$_{24}$-GE11/LUC or bisDBCO-PEG$_{24}$-GE11/LUC) were applied. The EGFR-specific antibody cetuximab (Erbitux, Merck, Darmstadt, Germany) was added in different concentrations (0.5, 1.5, 2.5, and 3.5 mg/mL) 15 min before the cell treatment with monoDBCO-PEG$_{24}$-GE11/NIS polyplexes. Furthermore, the NIS-specific inhibitor perchlorate (1 mM potassium perchlorate; Merck) was added as an additional control. At 24 h after transfection, NIS-mediated ^{125}I uptake was examined as described previously.[10,14] Results are normalized to cell survival and specified as counts per minute (cpm)/A620 (for cell viability assay, see below).

Cell viability assay

A commercially available 3-(4,5-dimethylthiazol-2-yl)-2,5-diphenyltetrazolium bromide (MTT) reagent (Sigma Aldrich) was added 24 h after transfection and cells were incubated for 1 h at 37°C. For cell lysis, 10% dimethyl sulfoxide in isopropanol with an incubation time of 15 min at room temperature was used. The measurement was performed on a Sunrise microplate absorbance reader (Tecan, Männedorf, Switzerland) at a wavelength of 620 nm.

Establishment of intracranial U87 tumors *in vivo*

Six- to 7-week-old female CD-1 nu/nu mice (Charles River, Sulzfeld, Germany) were anesthetized and immobilized, and a skin incision was made on the top of the skull. Mice were mounted onto a stereotactic head holder (David Kopf Instruments, Tujunga, CA) in the flat-skull position. A hole was carefully drilled into the skullcap 1.0 mm anterior and 1.5 mm lateral to the bregma with a 21G cannula. A blunt syringe with an injection volume of 1 μL (22G Hamilton syringe; Hamilton, Reno, NV) was inserted 4 mm deep and retracted to 3 mm depth. We injected 1 μL U87 cell suspension (1×10^5 cells/μL PBS) slowly (over 2 min) into the brain before the syringe was removed carefully within 2 further minutes. The area of injection was the right caudate putamen. The skin incision was stitched with surgical thread (Johnson & Johnson, New Brunswick, NJ) and the mice were kept warm while awakening. Mice were treated with Metacam (0.5 mg/kg) pre- and post-operatively to reduce pain and the risk of inflammation. Animals were maintained with access to mouse chow and water *ad libitum* and under specific-pathogen-free conditions. More than 15% weight loss or signs of ill health (impairment of breathing, drinking, eating, or cleaning behavior) led to sacrifice. All experimental protocols were authorized by the regional governmental commission for animals (Regierung von Oberbayern) and meet the requirements of the German Animal Welfare Act.

In vivo PET imaging studies after systemic *NIS* gene transfer

At 3.5–4 weeks after i.c. tumor cell inoculation, polyplexes (monoDBCO-PEG_{24}-GE11/NIS and bisDBCO-PEG_{24}-GE11/NIS polyplexes for EGFR targeting, non-targeted monoDBCO-PEG_{24}/NIS and bisDBCO-PEG_{24}/NIS polyplexes, monoDBCO-PEG_{24}-GE11/LUC and bisDBCO-PEG_{24}-GE11/LUC containing pCMVLuc as additional negative control) with a DNA dose of 2.5 mg/kg (for a 20-g mouse, 50 μg DNA in a total volume of 250 μL; solvent, HBG) were applied systemically via the tail vein. After 24 or 48 h, mice received 10 MBq of ^{124}I (PerkinElmer, Waltham, MA, or DSD Pharma, Purkersdorf, Austria) as an NIS PET tracer by i.v. injection, and NIS-mediated iodide accumulation in tumor areas was determined by small-animal PET (Inveon, SIEMENS Preclinical Solutions, Erlangen, Germany). Serial scanning took place 1, 3, and 5 h after ^{124}I application. Results were assessed with the software Inveon Acquisition Workplace (Siemens, Munich, Germany), were analyzed using Inveon Research Workplace (Siemens), and are represented as a percentage of the injected dose per milliliter tumor (% ID/mL). Mice were pretreated with L-thyroxine (LT4; 5 mg/mL, Sigma Aldrich) in their drinking water 10 days before imaging to reduce thyroidal iodide uptake, and at the same time the mouse chow was changed to a low-iodine diet (ssniff Spezialdiäten GmbH, Soest, Germany).

Mouse brain tissue preparation

After anesthesia and thorax incision, mice were perfused transcardially with 1× PBS followed by a 4% formaldehyde solution. The brain was explanted and fixed in 4% formaldehyde solution for 48 h at room temperature and stored in 1× PBS at 4°C for further preparation. The liver, spleen, kidney, and lungs were collected as control organs under the same procedure.

Immunohistochemical EGFR staining

Immunohistochemistry of tumor tissues derived from mice used for the imaging study was performed using a Bond RXm system (Leica, Wetzlar, Germany; all reagents from Leica) with an EGFR antibody (clone E235, 1:100, ab32077; Abcam). Briefly, slides were deparaffinized and pretreated with Epitope retrieval solution 1 (EDTA buffer [pH 6]) before the diluted primary antibody was applied for 15 min. Antibody binding was detected with a polymer refine detection kit without a post primary agent and visualized with diaminobenzidine as a dark brown precipitate. Counterstaining was done with hematoxylin. A positive control was included in each run. The stained slides were scanned with an automated slide scanner (Leica Biosystems; AT-2), and the Aperio Imagescope software (version 12.3; Leica Biosystems) was used to take representative images. The receptor expression level was evaluated by a veterinary pathologist.

Tumor volume estimation *ex vivo*

Tumors were cut in axial sections with a microtome. Twenty transverse layers with defined anatomical characteristics were selected with the help of a mouse brain atlas.[70] The interval between selected brain sections was 0.32–0.52 mm. Hematoxylin and eosin (H&E) staining was performed according to standard protocol, slides were scanned, all sections containing tumor were taken into consideration, and the tumor area (A) was determined by encircling the tumor (Aperio Imagescope software). The average area was calculated ($A_{average} = A_{total}/N$ [number of selected sections]) and the height of the tumor (H) was considered as the interval between the first and the last section containing tumor. The final tumor volume (in cubic millimeters) is the multiplication of $A_{average}$ (in square millimeters) and H (in millimeters).[71]

Only mice bearing a GBM with a size of >30 mm^3 were considered in the *in vivo* PET imaging studies. There was no significant difference in the mean tumor sizes between control and experimental groups: the groups that received targeted polyplexes had a mean tumor size of 44.6 ± 5.1 mm^3 (monoDBCO-PEG_{24}-GE11/NIS 48 h), 51.2 ± 6.0 mm^3 (monoDBCO-PEG_{24}-GE11/NIS 24 h), and 57.6 ± 8.6 mm^3 (bisDBCO-PEG_{24}-GE11/NIS), while those treated with non-targeted polyplexes developed tumors 43.9 ± 2.9 mm^3 (monoDBCO-PEG_{24}/NIS) and 43.9 ± 6.2 mm^3 (bisDBCO-PEG_{24}/NIS) in size. Animals treated with LUC-coding polyplexes had tumors with a mean size of 71.5 ± 10.0 mm^3 (monoDBCO-PEG_{24}-GE11/LUC) and 42.7 ± 8.9 mm^3 (bisDBCO-PEG_{24}-GE11/LUC).

Immunohistochemical staining of NIS protein

Paraffin-embedded tumor and control organ samples were immunohistochemically stained as described previously.[72] A primary mouse monoclonal NIS-specific antibody (Merck Millipore; dilution 1:500) was incubated on tissue samples for 60 min at room temperature, followed by a biotin-SP-conjugated goat antimouse IgG antibody (Jackson ImmunoResearch, West Grove, PA; dilution 1:200) for 20 min and peroxidase-conjugated streptavidin (Jackson ImmunoResearch; dilution 1:300) for a further 20 min. Scanning was performed as described above.

Radioiodide therapy study *in vivo*

Starting 5 days after i.c. tumor cell inoculation, tumor growth was assessed twice a week by high- resolution MRI. A visible tumor in one slice with a diameter between 0.8 and 1.3 mm was used as inclusion parameter (day 0). Therapy trials were started the day after. To this end, therapy mice were treated systemically with monoDBCO-PEG_{24}-GE11/NIS followed by an i.p. injection of 55.5 MBq ^{131}I (GE Healthcare, Braunschweig, Germany) 48 h later. The therapy trial was repeated three times; thus, i.v. polyplex injection took place on days 1, 5, and 9 and i.p. ^{131}I injections were performed on days 3, 7, and 11. Accordingly, control mice received monoDBCO-PEG_{24}/NIS followed by ^{131}I or monoDBCO-PEG_{24}-GE11/NIS followed by saline (NaCl), or NaCl i.v. followed by NaCl i.p., respectively. Once at least one endpoint criterion was met (>15% weight loss; impairment of breathing, drinking, eating, or cleaning behavior; self-isolation from the group), as monitored by independent animal care personnel blind to treatment and hypothesis, the mice were sacrificed.

MRI was acquired with a small animal 7T preclinical scanner (Agilent Discovery MR901 magnet and gradient system, Bruker AVANCE III HD electronics running ParaVision software release 6.0.1). A

birdcage quadrature volume resonator (inner diameter 72 mm; RAPID Biomedical, Rimpar, Germany) was used for 300 MHz RF transmission, and a rigid-housing two-channel surface receiver coil array (RAPID Biomedical) was placed over the mouse's head. Animals were screened for tumor growth with a T2-weighted rapid acquisition with relaxation enhancement (RARE) sequence, with a repetition time of 2.5 s, an effective echo time of 40 ms, 8 echoes per excitation, an acquisition matrix 192 × 192, an in-plane resolution of 0.104 × 0.104 mm^2, 1 average, and 7 slices with a thickness of 1 mm. The oblique coronal (horizontal) slices were tilted to be parallel with the brain anterior-posterior axis, which was tilted anterior-down due to mouse positioning under the coil. Images were exported in a Digital Imaging and Communications in Medicine (DICOM) format for analysis with the DICOM viewer RadiAnt (Medixant, Poznan, Poland). The tumor area of each slice was encircled and RadiAnt provided the size in square millimeters. The tumor volume was calculated using the same formula as for *ex vivo* tumor volume estimation (see above).

Ex vivo immunofluorescence assay

The U87 GBMs from therapy mice were prepared as described above. Two days after post-fixation in paraformaldehyde (PFA), the brains were left in 30% sucrose for at least 24 h at 4°C. Freezing was performed by embedding the tissue in Cryomatrix (Leica). Frozen tumor sections were stained with an antibody against Ki67 (Abcam; dilution 1:200) for cell proliferation and CD31 (BD Pharmingen, Heidelberg, Germany; dilution 1:100) for blood vessel density as described previously.[34] The stained tumor sections were scanned with the Pannoramic MIDI digital slide scanner and pictures were taken using Caseviewer software (3DHISTECH Ltd., Budapest, Hungary). For quantification, four visual fields (20× magnification) per tumor were chosen and analyzed with ImageJ software (NIH, Bethesda, MD).

Statistical methods

All *in vitro* experiments were performed at least in triplicate and results are shown as mean ± SEM, mean fold change ±SEM, and percentage for survival plots. Two-tailed Student's t test was used to prove statistical significance.

For therapy studies, differences in tumor growth were tested by one-way ANOVA followed by *post hoc* Fisher's LSD or Games Howell. Mouse survival is presented in a Kaplan-Meier-plot and statistical significance was tested by log rank. Statistical significance was defined as a p value of <0.05 (*$p < 0.05$; **$p < 0.01$; ***$p < 0.001$).

ACKNOWLEDGEMENTS

The authors want to thank Sissy M. Jhiang (Ohio State University, Columbus, OH, USA) for supplying the full-length human NIS cDNA. We owe special thanks to Sybille Reder, Markus Mittelhäuser, Hannes Rolbieski, Sandra Sühnel, Dr Geoffrey Topping, and Jakob Allmann (Department of Nuclear Medicine, Klinikum rechts der Isar, Technical University of Munich, Munich, Germany) for their assistance and support in performing the imaging and therapy studies. We are grateful to Olga Seelbach and her team (Institute of Pathology, School of Medicine, Technical University of Munich, Munich, Germany) for the preparation of paraffin-embedded slides and the H&E and EGFR staining. We appreciate the help from Prof. Dr. Gabriele Multhoff and Dr. Stefan Stangl (Center for Translational Cancer Research, Klinikum rechts der Isar, Technical University of Munich, Munich, Germany) for establishing the orthotopic glioblastoma mouse model in our group. Furthermore, we thank Prof. Dr. Julia Mayerle, Dr. Ivonne Regel, and Dr. Ujjwal Mahajan for allowing us to use their laboratory equipment.

This work was supported by a grant from the Deutsche Forschungsgemeinschaft within the Collaborative Research Center SFB 824 to C.S. (project C8) and to F.S. (project Z3), and SFB 1032 to E.W. (project B4), as well as within the Priority Program SPP1629 to C.S. and P.J.N., and by a grant form the Wilhelm Sander-Stiftung to C.S. and P.J.N. (2014.129.1). R.G. and R.E.K. gratefully acknowledge funding by the DFG (GL691/2; SFB824-B2) and the Anni-Hofmann Stiftung.

This work was performed as partial fulfillment of the doctoral thesis of R.S. at the Faculty for Chemistry and Pharmacy of the LMU Munich.

AUTHOR CONTRIBUTIONS

Conceptualization: R.S., K.A.S., S.B., R.G., E.W., P.J.N., and C.S.; methodology: R.S., T.B.-H., S.B., R.E.K., E.W., P.J.N., and C.S.; investigation: R.S., T.B.-H., C.K., N.S., and H.Y.; formal analysis: R.S., H.Y., and C.Z.; resources: F.S., W.A.W., and R.G.; writing – original manuscript: R.S.; writing – review & editing: T.B.-H., S.B., K.A.S., R.E.K., E.W., P.J.N., and C.S.; funding acquisition: E.W., P.J.N., and C.S.; supervision: E.W. and C.S.

DECLARATION OF INTERESTS

The authors have declared no conflict of interest.

REFERENCES

1. Aum, D.J., Kim, D.H., Beaumont, T.L., Leuthardt, E.C., Dunn, G.P., and Kim, A.H. (2014). Molecular and cellular heterogeneity: the hallmark of glioblastoma. Neurosurg. Focus *37*, E11.

2. Louis, D.N., Perry, A., Reifenberger, G., von Deimling, A., Figarella-Branger, D., Cavenee, W.K., Ohgaki, H., Wiestler, O.D., Kleihues, P., and Ellison, D.W. (2016). The 2016 world health organization classification of tumors of the central nervous system: a summary. Acta Neuropathol. *131*, 803–820.

3. Bastien, J.I.L., McNeill, K.A., and Fine, H.A. (2015). Molecular characterizations of glioblastoma, targeted therapy, and clinical results to date. Cancer *121*, 502–516.

4. Aldape, K., Brindle, K.M., Chesler, L., Chopra, R., Gajjar, A., Gilbert, M.R., Gottardo, N., Gutmann, D.H., Hargrave, D., Holland, E.C., et al. (2019). Challenges to curing primary brain tumours. Nat. Rev. Clin. Oncol. *16*, 509–520.

5. Ginn, S.L., Amaya, A.K., Alexander, I.E., Edelstein, M., and Abedi, M.R. (2018). Gene therapy clinical trials worldwide to 2017: an update. J. Gene Med. *20*, e3015.

6. Spitzweg, C., and Morris, J.C. (2002). The sodium iodide symporter: its pathophysiological and therapeutic implications. Clin. Endocrinol. *57*, 559–574.

7. Penheiter, A.R., Russell, S.J., and Carlson, S.K. (2012). The sodium iodide symporter (NIS) as an imaging reporter for gene, viral, and cell-based therapies. Curr. Gene Ther. *12*, 33–47.

8. Urnauer, S., Müller, A.M., Schug, C., Schmohl, K.A., Tutter, M., Schwenk, N., Rödl, W., Morys, S., Ingrisch, M., Bertram, J., et al. (2017). EGFR-targeted nonviral NIS

gene transfer for bioimaging and therapy of disseminated colon cancer metastases. Oncotarget *8*, 92195–92208.

9. Smanik, P.A., Liu, Q., Furminger, T.L., Ryu, K., Xing, S., Mazzaferri, E.L., and Jhiang, S.M. (1996). Cloning of the human sodium iodide symporter. Biochem. Biophys. Res. Commun. *226*, 339–345.
10. Willhauck, M.J., Sharif Samani, B.R., Gildehaus, F.J., Wolf, I., Senekowitsch-Schmidtke, R., Stark, H.J., Göke, B., Morris, J.C., and Spitzweg, C. (2007). Application of 188rhenium as an alternative radionuclide for treatment of prostate cancer after tumor-specific sodium iodide symporter gene expression. J. Clin. Endocrinol. Metab. *92*, 4451–4458.
11. Spitzweg, C. (2009). Gene therapy in thyroid cancer. Horm. Metab. Res. *41*, 500–509.
12. Spitzweg, C., Dietz, A.B., O'Connor, M.K., Bergert, E.R., Tindall, D.J., Young, C.Y., and Morris, J.C. (2001). In vivo sodium iodide symporter gene therapy of prostate cancer. Gene Ther. *8*, 1524–1531.
13. Spitzweg, C., O'Connor, M.K., Bergert, E.R., Tindall, D.J., Young, C.Y., and Morris, J.C. (2000). Treatment of prostate cancer by radioiodine therapy after tissue-specific expression of the sodium iodide symporter. Cancer Res. *60*, 6526–6530.
14. Spitzweg, C., Zhang, S., Bergert, E.R., Castro, M.R., McIver, B., Heufelder, A.E., Tindall, D.J., Young, C.Y., and Morris, J.C. (1999). Prostate-specific antigen (PSA) promoter-driven androgen-inducible expression of sodium iodide symporter in prostate cancer cell lines. Cancer Res. *59*, 2136–2141.
15. Amer, M.H. (2014). Gene therapy for cancer: present status and future perspective. Mol. Cell. Ther. *2*, 27.
16. Knoop, K., Kolokythas, M., Klutz, K., Willhauck, M.J., Wunderlich, N., Draganovici, D., Zach, C., Gildehaus, F.J., Böning, G., Göke, B., et al. (2011). Image-guided, tumor stroma-targeted 131I therapy of hepatocellular cancer after systemic mesenchymal stem cell-mediated NIS gene delivery. Mol. Ther. *19*, 1704–1713.
17. Knoop, K., Schwenk, N., Dolp, P., Willhauck, M.J., Zischek, C., Zach, C., Hacker, M., Göke, B., Wagner, E., Nelson, P.J., et al. (2013). Stromal targeting of sodium iodide symporter using mesenchymal stem cells allows enhanced imaging and therapy of hepatocellular carcinoma. Hum. Gene Ther. *24*, 306–316.
18. Knoop, K., Schwenk, N., Schmohl, K., Müller, A., Zach, C., Cyran, C., Carlsen, J., Böning, G., Bartenstein, P., Göke, B., et al. (2015). Mesenchymal stem cell-mediated, tumor stroma-targeted radioiodine therapy of metastatic colon cancer using the sodium iodide symporter as theranostic gene. J. Nucl. Med. *56*, 600–606.
19. Schug, C., Gupta, A., Urnauer, S., Steiger, K., Cheung, P.F., Neander, C., Savvatakis, K., Schmohl, K.A., Trajkovic-Arsic, M., Schwenk, N., et al. (2019). A novel approach for image-guided (131)I therapy of pancreatic ductal adenocarcinoma using mesenchymal stem cell-mediated NIS gene delivery. Mol. Cancer Res. *17*, 310–320.
20. Schug, C., Kitzberger, C., Sievert, W., Spellerberg, R., Tutter, M., Schmohl, K.A., Eberlein, B., Biedermann, T., Steiger, K., Zach, C., et al. (2019). Radiation-induced amplification of TGFB1-induced mesenchymal stem cell-mediated sodium iodide symporter (NIS) gene (131)I therapy. Clin. Cancer Res. *25*, 5997–6008.
21. Schug, C., Sievert, W., Urnauer, S., Müller, A.M., Schmohl, K.A., Wechselberger, A., Schwenk, N., Lauber, K., Schwaiger, M., Multhoff, G., et al. (2018). External beam radiation therapy enhances mesenchymal stem cell-mediated sodium-iodide symporter gene delivery. Hum. Gene Ther. *29*, 1287–1300.
22. Schug, C., Urnauer, S., Jaeckel, C., Schmohl, K.A., Tutter, M., Steiger, K., Schwenk, N., Schwaiger, M., Wagner, E., Nelson, P.J., et al. (2019). TGFB1-driven mesenchymal stem cell-mediated NIS gene transfer. Endocr. Relat. Cancer *26*, 89–101.
23. Müller, A.M., Schmohl, K.A., Knoop, K., Schug, C., Urnauer, S., Hagenhoff, A., Clevert, D.A., Ingrisch, M., Niess, H., Carlsen, J., et al. (2016). Hypoxia-targeted 131I therapy of hepatocellular cancer after systemic mesenchymal stem cell-mediated sodium iodide symporter gene delivery. Oncotarget *7*, 54795–54810.
24. Tutter, M., Schug, C., Schmohl, K.A., Urnauer, S., Schwenk, N., Petrini, M., Lokerse, W.J.M., Zach, C., Ziegler, S., Bartenstein, P., et al. (2020). Effective control of tumor growth through spatial and temporal control of theranostic sodium iodide symporter (NIS) gene expression using a heat-inducible gene promoter in engineered mesenchymal stem cells. Theranostics *10*, 4490–4506.
25. Tutter, M., Schug, C., Schmohl, K.A., Urnauer, S., Kitzberger, C., Schwenk, N., Petrini, M., Zach, C., Ziegler, S., Bartenstein, P., et al. (2021). Regional hyperthermia enhances mesenchymal stem cell recruitment to tumor stroma: implications for mesenchymal stem cell-based tumor therapy. Mol. Ther. *29*, 788–803.
26. Klutz, K., Russ, V., Willhauck, M.J., Wunderlich, N., Zach, C., Gildehaus, F.J., Göke, B., Wagner, E., Ogris, M., and Spitzweg, C. (2009). Targeted radioiodine therapy of neuroblastoma tumors following systemic nonviral delivery of the sodium iodide symporter gene. Clin. Cancer Res. *15*, 6079–6086.
27. Klutz, K., Willhauck, M.J., Dohmen, C., Wunderlich, N., Knoop, K., Zach, C., Senekowitsch-Schmidtke, R., Gildehaus, F.J., Ziegler, S., Fürst, S., et al. (2011). Image-guided tumor-selective radioiodine therapy of liver cancer after systemic nonviral delivery of the sodium iodide symporter gene. Hum. Gene Ther. *22*, 1563–1574.
28. Schmohl, K.A., Dolp, P., Schug, C., Knoop, K., Klutz, K., Schwenk, N., Bartenstein, P., Nelson, P.J., Ogris, M., Wagner, E., et al. (2017). Reintroducing the sodium-iodide symporter to anaplastic thyroid carcinoma. Thyroid *27*, 1534–1543.
29. Klutz, K., Schaffert, D., Willhauck, M.J., Grünwald, G.K., Haase, R., Wunderlich, N., Zach, C., Gildehaus, F.J., Senekowitsch-Schmidtke, R., Göke, B., et al. (2011). Epidermal growth factor receptor-targeted (131)I-therapy of liver cancer following systemic delivery of the sodium iodide symporter gene. Mol. Ther. *19*, 676–685.
30. Schmohl, K.A., Gupta, A., Grünwald, G.K., Trajkovic-Arsic, M., Klutz, K., Braren, R., Schwaiger, M., Nelson, P.J., Ogris, M., Wagner, E., et al. (2017). Imaging and targeted therapy of pancreatic ductal adenocarcinoma using the theranostic sodium iodide symporter (NIS) gene. Oncotarget *8*, 33393–33404.
31. Schäfer, A., Pahnke, A., Schaffert, D., van Weerden, W.M., de Ridder, C.M.A., Rödl, W., et al. (2011). Disconnecting the yin and yang relation of epidermal growth factor receptor (EGFR)-mediated delivery: a fully synthetic, EGFR-targeted gene transfer system avoiding receptor activation. Hum. Gene Ther. *22*, 1463–1473.
32. Urnauer, S., Klutz, K., Grünwald, G.K., Morys, S., Schwenk, N., Zach, C., Gildehaus, F.J., Rödl, W., Ogris, M., Wagner, E., et al. (2017). Systemic tumor-targeted sodium iodide symporter (NIS) gene therapy of hepatocellular carcinoma mediated by B6 peptide polyplexes. J. Gene Med. *19*, e2957.
33. Urnauer, S., Morys, S., Krhac Levacic, A., Müller, A.M., Schug, C., Schmohl, K.A., Schwenk, N., Zach, C., Carlsen, J., Bartenstein, P., et al. (2016). Sequence-defined cMET/HGFR-targeted polymers as gene delivery vehicles for the theranostic sodium iodide symporter (NIS) gene. Mol. Ther. *24*, 1395–1404.
34. Urnauer, S., Schmohl, K.A., Tutter, M., Schug, C., Schwenk, N., Morys, S., Ziegler, S., Bartenstein, P., Clevert, D.A., Wagner, E., et al. (2019). Dual-targeted NIS polyplexes-a theranostic strategy toward tumors with heterogeneous receptor expression. Gene Ther. *26*, 93–108.
35. Lächelt, U., and Wagner, E. (2015). Nucleic acid therapeutics using polyplexes: a journey of 50 Years (and beyond). Chem. Rev. *115*, 11043–11078.
36. Klein, P.M., Kern, S., Lee, D.J., Schmaus, J., Höhn, M., Gorges, J., Kazmaier, U., and Wagner, E. (2018). Folate receptor-directed orthogonal click-functionalization of siRNA lipopolyplexes for tumor cell killing in vivo. Biomaterials *178*, 630–642.
37. Hager, S., and Wagner, E. (2018). Bioresponsive polyplexes - chemically programmed for nucleic acid delivery. Expert Opin. Drug Deliv. *15*, 1067–1083.
38. Ogris, M., Brunner, S., Schüller, S., Kircheis, R., and Wagner, E. (1999). PEGylated DNA/transferrin-PEI complexes: reduced interaction with blood components, extended circulation in blood and potential for systemic gene delivery. Gene Ther. *6*, 595–605.
39. Wang, S., Reinhard, S., Li, C., Qian, M., Jiang, H., Du, Y., Lächelt, U., Lu, W., Wagner, E., and Huang, R. (2017). Antitumoral cascade-targeting ligand for IL-6 receptor-mediated gene delivery to glioma. Mol. Ther. *25*, 1556–1566.
40. Kos, P., Lächelt, U., He, D., Nie, Y., Gu, Z., and Wagner, E. (2015). Dual-targeted polyplexes based on sequence-defined peptide-PEG-oligoamino amides. J. Pharm. Sci. *104*, 464–475.
41. Li, Z., Zhao, R., Wu, X., Sun, Y., Yao, M., Li, J., Xu, Y., and Gu, J. (2005). Identification and characterization of a novel peptide ligand of epidermal growth factor receptor for targeted delivery of therapeutics. FASEB J. *19*, 1978–1985.
42. Rao, S.A., Arimappamagan, A., Pandey, P., Santosh, V., Hegde, A.S., Chandramouli, B.A., and Somasundaram, K. (2013). miR-219-5p inhibits receptor tyrosine kinase pathway by targeting EGFR in glioblastoma. PloS one *8*, e63164.
43. Eskilsson, E., Røsland, G.V., Solecki, G., Wang, Q., Harter, P.N., Graziani, G., et al. (2018). EGFR heterogeneity and implications for therapeutic intervention in glioblastoma. Neuro oncol. *20*, 743–752.

44. Mickler, F.M., Möckl, L., Ruthardt, N., Ogris, M., Wagner, E., and Bräuchle, C. (2012). Tuning nanoparticle uptake: live-cell imaging reveals two distinct endocytosis mechanisms mediated by natural and artificial EGFR targeting ligand. Nano Lett. *12*, 3417–3423.

45. Wang, Y., Luo, J., Truebenbach, I., Reinhard, S., Klein, P.M., Höhn, M., Kern, S., Morys, S., Loy, D.M., Wagner, E., et al. (2020). Double click-functionalized siRNA polyplexes for gene silencing in epidermal growth factor receptor-positive tumor cells. ACS Biomater. Sci. Eng. *6*, 1074–1089.

46. Morys, S., Urnauer, S., Spitzweg, C., and Wagner, E. (2018). EGFR targeting and shielding of pDNA lipopolyplexes via bivalent attachment of a sequence-defined PEG agent. Macromol. Biosci. *18*, 1700203.

47. Truebenbach, I., Zhang, W., Wang, Y., Kern, S., Höhn, M., Reinhard, S., Gorges, J., Kazmaier, U., and Wagner, E. (2019). Co-delivery of pretubulysin and siEG5 to EGFR overexpressing carcinoma cells. Int. J. Pharm. *569*, 118570.

48. Steinborn, B., Truebenbach, I., Morys, S., Lächelt, U., Wagner, E., and Zhang, W. (2018). Epidermal growth factor receptor targeted methotrexate and small interfering RNA co-delivery. J. Gene Med. *20*, e3041.

49. Jo, D.H., Kim, J.H., Lee, T.G., and Kim, J.H. (2015). Size, surface charge, and shape determine therapeutic effects of nanoparticles on brain and retinal diseases. Nanomedicine *11*, 1603–1611.

50. Boeckle, S., von Gersdorff, K., van der Piepen, S., Culmsee, C., Wagner, E., and Ogris, M. (2004). Purification of polyethylenimine polyplexes highlights the role of free polycations in gene transfer. J. Gene Med. *6*, 1102–1111.

51. Batash, R., Asna, N., Schaffer, P., Francis, N., and Schaffer, M. (2017). Glioblastoma multiforme, diagnosis and treatment; recent literature review. Curr. Med. Chem. *24*, 3002–3009.

52. Šamec, N., Zottel, A., Videtič Paska, A., and Jovčevska, I. (2020). Nanomedicine and immunotherapy: a step further towards precision medicine for glioblastoma. Molecules *25*, 490.

53. Rajesh, Y., Pal, I., Banik, P., Chakraborty, S., Borkar, S.A., Dey, G., Mukherjee, A., and Mandal, M. (2017). Insights into molecular therapy of glioma: current challenges and next generation blueprint. Acta Pharmacol. Sin. *38*, 591–613.

54. Pruitt, A.A., and Rosenfeld, M.R. (2005). 10 questions about temozolomide and the treatment of brain tumors. The Neurol. *11*, 362–365.

55. Zhao, M., van Straten, D., Broekman, M.L.D., Préat, V., and Schiffelers, R.M. (2020). Nanocarrier-based drug combination therapy for glioblastoma. Theranostics *10*, 1355–1372.

56. Dai, G., Levy, O., and Carrasco, N. (1996). Cloning and characterization of the thyroid iodide transporter. Nature *379*, 458–460.

57. Baril, P., Martin-Duque, P., and Vassaux, G. (2010). Visualization of gene expression in the live subject using the Na/I symporter as a reporter gene: applications in biotherapy. Br. J. Pharmacol. *159*, 761–771.

58. Li, H., Nakashima, H., Decklever, T.D., Nace, R.A., and Russell, S.J. (2013). HSV-NIS, an oncolytic herpes simplex virus type 1 encoding human sodium iodide symporter for preclinical prostate cancer radiovirotherapy. Cancer Gene Ther. *20*, 478–485.

59. Spitzweg, C., Harrington, K.J., Pinke, L.A., Vile, R.G., and Morris, J.C. (2001). Clinical review 132: the sodium iodide symporter and its potential role in cancer therapy. J. Clin. Endocrinol. Metab. *86*, 3327–3335.

60. Cho, J.Y., Xing, S., Liu, X., Buckwalter, T.L., Hwa, L., Sferra, T.J., Chiu, I.M., and Jhiang, S.M. (2000). Expression and activity of human Na+/I- symporter in human glioma cells by adenovirus-mediated gene delivery. Gene Ther. *7*, 740–749.

61. Opyrchal, M., Allen, C., Iankov, I., Aderca, I., Schroeder, M., Sarkaria, J., and Galanis, E. (2012). Effective radiovirotherapy for malignant gliomas by using oncolytic measles virus strains encoding the sodium iodide symporter (MV-NIS). Hum. Gene Ther. *23*, 419–427.

62. Zhang, P., and Wagner, E. (2017). History of polymeric gene delivery systems. Top. Curr. Chem. *375*, 26.

63. Berger, S., Krhač Levačić, A., Hörterer, E., Wilk, U., Benli-Hoppe, T., Wang, Y., Öztürk, Ö., Luo, J., and Wagner, E. (2021). Optimizing pDNA lipo-polyplexes: a balancing act between stability and cargo release. Biomacromolecules *22*, 1282–1296.

64. Klutz, K., Willhauck, M.J., Wunderlich, N., Zach, C., Anton, M., Senekowitsch-Schmidtke, R., Göke, B., and Spitzweg, C. (2011). Sodium iodide symporter (NIS)-mediated radionuclide ((131)I, (188)Re) therapy of liver cancer after transcriptionally targeted intratumoral in vivo NIS gene delivery. Hum. Gene Ther. *22*, 1403–1412.

65. Willhauck, M.J., Sharif-Samani, B., Senekowitsch-Schmidtke, R., Wunderlich, N., Göke, B., Morris, J.C., and Spitzweg, C. (2008). Functional sodium iodide symporter expression in breast cancer xenografts in vivo after systemic treatment with retinoic acid and dexamethasone. Breast Cancer Res. Treat. *109*, 263–272.

66. Spitzweg, C., Nelson, P.J., Wagner, E., Bartenstein, P., Weber, W.A., Schwaiger, M., and Morris, J.C. (2021). The sodium iodide symporter (NIS): novel applications for radionuclide imaging and treatment. Endocr. Relat. Cancer *28*, T193–T213.

67. Frisch, A., Kälin, S., Monk, R., Radke, J., Heppner, F.L., and Kälin, R.E. (2020). Apelin controls angiogenesis-dependent glioblastoma growth. Int. J. Mol. Sci. *21*, 4179.

68. van den Bent, M.J., Gao, Y., Kerkhof, M., Kros, J.M., Gorlia, T., van Zwieten, K., Prince, J., van Duinen, S., Sillevis Smitt, P.A., Taphoorn, M., et al. (2015). Changes in the EGFR amplification and EGFRvIII expression between paired primary and recurrent glioblastomas. Neuro Oncol. *17*, 935–941.

69. Plank, C., Zatloukal, K., Cotten, M., Mechtler, K., and Wagner, E. (1992). Gene transfer into hepatocytes using asialoglycoprotein receptor mediated endocytosis of DNA complexed with an artificial tetra-antennary galactose ligand. Bioconjug. Chem. *3*, 533–539.

70. Franklin, K.B., and Paxinos, G. (2019). Paxinos and Franklin's the Mouse Brain in Stereotaxic Coordinates, Compact: The Coronal Plates and Diagrams (Academic press).

71. Kälin, R.E., Cai, L., Li, Y., Zhao, D., Zhang, H., Cheng, J., et al. (2021). TAMEP are brain tumor parenchymal cells controlling neoplastic angiogenesis and progression. Cell Syst. *12*, 248–262.e7.

72. Spitzweg, C., Baker, C.H., Bergert, E.R., O'Connor, M.K., and Morris, J.C. (2007). Image-guided radioiodide therapy of medullary thyroid cancer after carcinoembryonic antigen promoter-targeted sodium iodide symporter gene expression. Hum. Gene Ther. *18*, 916–924.